Dispersion engineering in a Brillouin fiber laser cavity for Kerr frequency comb formation

Moise Deroh, Erwan Lucas, Bertrand Kibler

Dispersion engineering in Brillouin fiber laser cavity for Kerr frequency comb formation

MOISE DEROH[1,*], ERWAN LUCAS[1], AND BERTRAND KIBLER[1]

[1] Laboratoire Interdisciplinaire Carnot de Bourgogne, UMR 6303 CNRS, Université Bourgogne Franche-Comté (UBFC), Dijon, France
[*] Corresponding author: koffi.deroh@u-bourgogne.fr

Compiled December 20, 2023

We conduct numerical and experimental investigations on Kerr comb generation in a nonlinear and nonreciprocal fiber cavity by leveraging both stimulated Brillouin backscattering and cascaded four-wave mixing. By engineering the net cavity dispersion to be either normal or anomalous, we enable the formation of diverse patterns and localized structures in the cavity field. The comb's properties depend crucially on the mismatch between the frequency spacing of the bichromatic pump and the free spectral range of the Brillouin laser cavity in both cases. Particularly, in the anomalous regime, adjusting this parameter yields coherent, stable frequency combs in the modulation instability regime. This allows control and expansion of the spectral bandwidth up to 2 THz in normal dispersion and to 6 THz under anomalous net dispersion. This versatile and easily reconfigurable method holds potential for applications in high-speed communications and microwave synthesis.

http://dx.doi.org/10.1364/ao.XX.XXXXXX

1. INTRODUCTION

Optical frequency combs (OFCs), comprising a series of equally spaced coherent lines in the frequency domain, have found widespread use in a wide panel of applications encompassing optical frequency metrology, spectrograph calibration, microwave generation, and beyond [1]. OFCs originate from various sources, including mode-locked lasers [2], electro-optic modulation [3, 4], and passive nonlinear resonators [5]. The latter, using the formation of dissipative temporal cavity solitons in microresonators [6], generates smooth OFCs at high repetition rates, ideal for optical communications and LIDAR systems.

The pursuit of Kerr combs has not been confined to these traditional optical platforms. While early work on microresonators showed a competition between Kerr and Raman or Brillouin scattering [7], a novel approach has recently emerged, demonstrating the generation of soliton-based combs leveraging Brillouin lasing [8, 9]. In this paradigm, the Brillouin gain in the cavity gives rise to counterpropagating Brillouin lasing [10] that serves as the coherent driving force behind Kerr comb generation. This paradigm has been extended to fiber cavity Brillouin lasers under bichromatic pumping, to trigger Kerr comb formation at a high repetition rate while using a long cavity [11–13]. Intriguingly, this dual-pumping configuration bestows an additional degree of freedom for manipulating cavity dynamics, specifically the frequency mismatch between the comb repetition rate and the cavity's free spectral range (FSR) [14, 15], which had not been investigated so far in these systems.

In this letter, we investigate the intricate interplay between stimulated Brillouin scattering (SBS) and cascaded four-wave mixing (FWM) in the nonlinear fiber cavity, to achieve coherent and stabilized frequency combs. We experimentally study and numerically validate the impact of the frequency mismatch parameter on the comb dynamics, and specifically its spectral shape and bandwidth. In addition, we perform this analysis in both normal and anomalous group velocity dispersion regimes, since the net fiber cavity dispersion can be easily adjusted by inserting a short fiber segment in the cavity. In each case, the generation of switching waves or localized structures through modulation instability (MI), from the initial bichromatic sinusoidal modulation pattern, is investigated and characterized in the spectral and temporal domains.

2. EXPERIMENTAL SETUP AND RESULTS

Our experimental setup, depicted in fig. 1a, involves a cavity configuration that utilizes a highly nonlinear fiber (HNLF) with a length of 10 m, and standard single-mode fiber (SMF-28) components with a total length of 1.15 m, resulting in a normal net dispersion of $-0.94\,\mathrm{ps\,km^{-1}\,nm^{-1}}$. The dispersion and nonlinear parameters of the HNLF and SMF fibers used in our cavity at 1551.7 nm wavelength are $D = -2.95$ and $18\,\mathrm{ps\,km^{-1}\,nm^{-1}}$, $\beta_2 = 3.77$ and $-21.7\,\mathrm{ps^2\,km^{-1}}$, $\gamma = 12$ and $1.2\,\mathrm{W^{-1}\,km^{-1}}$. Introducing a 1 m long segment of SMF-28 shifts the cavity into the anomalous net dispersion regime ($\sim 0.5\,\mathrm{ps\,km^{-1}\,nm^{-1}}$). For both cases, the cavity finesse was determined to be approximately $f \sim 26$. The total roundtrip losses, primarily attributed to the circulator, amounted to 1.2 dB. Considering the overall length of the fiber cavity, the FSR of the cavity are 18.39 MHz and 16.9 MHz in the normal and anomalous net dispersion regimes, respectively. To generate two pump lines of equal power, we use an electro-optic method. A tunable narrow-linewidth continuous-wave laser centered at 1551.7 nm is intensity modulated at the null transmission point of an intensity modulator (IM) to create two controllable sidebands while suppressing the optical carrier wave. The frequency spacing of the

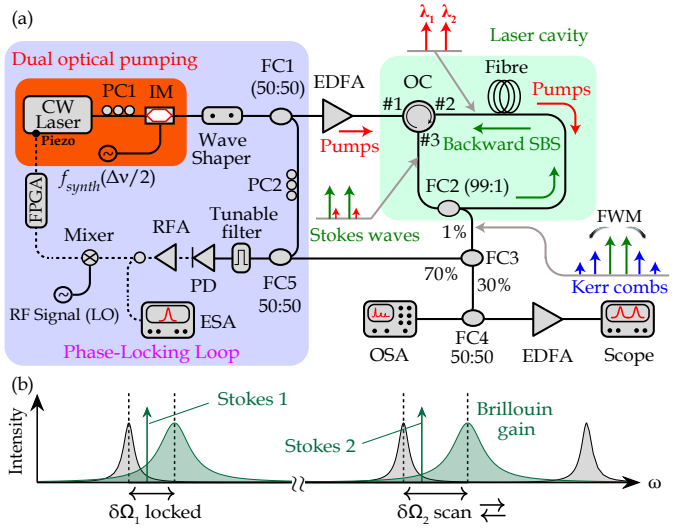

Fig. 1. **(a)** Experimental setup for Kerr combs generation in a dual-frequency Brillouin fiber laser cavity (green rectangle) benefiting from the phase-locked stabilization loop diagram (purple rectangle). CW: Continuous wave, PC: Polarization controller, IM: Intensity modulator, FC: Fiber coupler, EDFA: Erbium-doped fiber amplifier, OC: Optical circulator, SBS: Stimulated Brillouin scattering, FWM: Four wave mixing, OSA: Optical spectrum analyzer, PD: Photodiode, RFA: Radio frequency amplifier, ESA: Electrical spectrum analyzer, LO: Local oscillator, FPGA: Field-programmable gate array. **(b)** Principle of the offset sideband-locking for the Brillouin gain spectrum detuning scan.

pumps is set by the modulation frequency around $\Delta\nu \sim 40$ GHz and can be precisely tuned. A programmable optical filter is employed to further reject the residual carrier and any higher-order sidebands. The dual pump is then divided into two segments. The first segment is amplified using an erbium-doped fiber amplifier (EDFA) and introduced into the fiber cavity through an optical circulator (OC). These pumps undergo a single pass through the HNLF in the forward direction before being isolated by the OC. Simultaneously, two backscattered Stokes waves are generated, with a frequency down-shift of ∼9.1 GHz from the pump frequencies [16], corresponding to the acoustic phonon energy. Within the cavity, a 99:1 fiber tap coupler is inserted to extract and analyze the counterpropagating Brillouin laser signals. The remaining 99 % of the Stokes waves are recirculated back into the passive fiber ring cavity, resulting in the dual lasing effect that initiates a cascade of FWM and leads to the formation of Kerr combs. The second part of the bichromatic laser is recombined with a portion of the cavity's output, to create a beatnote between one of the Stokes laser and its pump. This beatnote is stabilized to a local oscillator via a digital phase-locking loop (PLL) which feeds back on the laser wavelength [17, 18], and compensates for the relative thermal drift between the fiber cavity and the pump laser. This PLL scheme locks the detuning of one of the Brillouin gain lobes relative to the cavity ($\delta\Omega_1$ in fig. 1b). Changing $f_{\text{synth}} = \Delta\nu/2$ hence controls $\delta\Omega_2$ and thereby the Stokes lasing frequency via the mode pulling effect [9]. An electrical spectrum analyzer (ESA) is used to monitor the pump beatnote, to ensure single-frequency operation of the Stokes laser. Note that the input polarization states were controlled via polarization controllers to maximize the extracted Brillouin lasing signal. Finally, spectral and temporal characterizations of the cavity output field are performed using a high-resolution optical spectrum analyzer (APEX Technologies AP2243B) and an optical sampling oscilloscope (EXFO PSO-101). To simulate the cavity system, we employ a specific model based on coupled equations derived from the Ikeda map and use a two-step approach for each roundtrip in the fiber cavity [19]. First, we compute the SBS steady state by solving the Brillouin master equations [20] numerically, and then we solve the modified Nonlinear Schrödinger Equation using the split-step Fourier method, accounting for Brillouin gain in the pumped Stokes modes, cavity recirculation and losses. Our model is benchmarked against the measurements and provides excellent agreement.

A. Normal dispersion regime

We first characterized the comb dynamics under net normal dispersion. Figures 2a,b report both measured and numerically simulated Kerr comb spectra, while tuning $\Delta\nu$ by changing the frequency modulation of the IM. Since one pump is effectively locked to a cavity mode via the PLL, its detuning is fixed, while that of the other pump is swept as a result. The total pump power is fixed at 430 mW. Spectral and temporal measurements are performed simultaneously during the frequency scan. Our results show that a mismatch between $\Delta\nu$ and the FSR-multiple of the laser cavity has a significant impact on both the spectral broadening and shape of the Kerr comb in such dispersion regime. Our numerical predictions show good agreement with the experimental data. As predicted in [19], the optimal pump frequency spacing, where the stable Kerr comb spectrum is the broadest, occurs when $\Delta\nu$ is commensurate with a multiple of the cavity FSR. This situation corresponds to an equal detuning for both pump lasers. We observed mode-hopping effects, as highlighted in fig. 2a depending on the detuning of the pumps. At these points, the lasing from a longitudinal mode switches to the adjacent one and the detuning of the tuned pump abruptly changes sign. Hence, mode hopping limits the achievable pumps detuning range. We could replicate this effect in simulations by wrapping the pump's detuning in the range $\pm$FSR/2 (see fig. 2b). Note that the FSR of the fiber cavity must be greater than the spontaneous Brillouin gain bandwidth (typically around 55 MHz [16] in our case) in order to avoid multimode Brillouin lasing [19]. The dual-frequency pump spacing and pump power were chosen to preserve a coherent single Brillouin frequency lasing emission while maximizing the Kerr comb spectral bandwidth. Figures 2c,d shows two distinct Kerr comb spectra from the previous maps. In both cases, our numerical predictions match the experimental data remarkably well. The first corresponds to the commensurate $\Delta\nu$ spacing case, and exhibits a symmetric shape of the comb with a maximum bandwidth around 2 THz at −60 dB. The other comb has an asymmetrical shape, which is caused by the unequal detuning of the pumps, which leads to a shift of the Kerr comb center frequency. In addition, we characterized these two combs in the time domain, as illustrated in fig. 2e which shows the temporal intensity profiles of the picosecond pulses corresponding to the combs in figs. 2c,d. They correspond to the formation of a switching wave [21] onto the sinusoidal modulation pattern induced by the interference between the two Stokes fields in the cavity. Our numerical prediction (fig. 2f) of the intracavity temporal intensity profile shows good agreement with the experimental data. In both cases, the measured temporal profiles follow the expected switching wavefront formation, i.e. a pulse train with a ∼25 ps period with flat-top pulses in the case of the symmetric Kerr comb (fig. 2e, blue curve). The pulse shape changes slightly

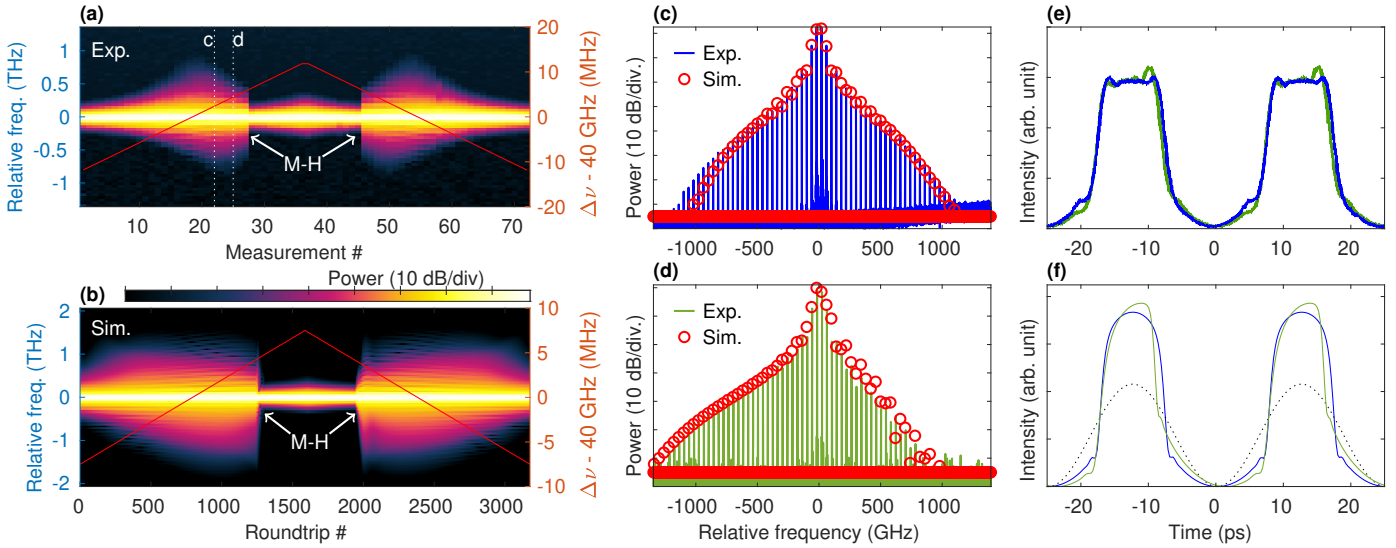

Fig. 2. Normal net dispersion regime. **(a)** Experimental recording of the comb evolution with $\Delta\nu$, at fixed injected optical power of 430 mW. M-H : Mode Hopping. **(b)** Simulated evolution of the comb spectrum when scanning the detuning of one pump. **(c)** Examples of symmetric comb in the scan in (a). The red circles show the numerical simulation. **(d)** Examples of asymmetric comb in the scan in (a) and comparison with simulations. **(e)** Experimental temporal intensity profiles of the generated pulse train corresponding to both cases reported in (c) and (d). **(f)** Numerical simulation of intra-cavity temporal intensity profile corresponding to the cases in (c) and (d). The dashed lines corresponds to the interference between the 2 Stokes lines.

when the comb shape is asymmetric (fig. 2e, green curve).

B. Anomalous dispersion regime

Next, we analyzed the cavity with net anomalous dispersion. The same previous set of measurements were performed, and the numerical simulations have been adapted to the new laser cavity parameters. Figure 3a shows the experimental evolution Kerr comb spectra when changing the detuning of one pump, when varying $\Delta\nu$, at fixed injected pump power of 535 mW. As in the net normal dispersion case, tuning this parameter significantly impacts the Kerr comb spectral shape and stability. A striking distinct feature of the anomalous dispersion regime is the formation of MI gain lobes [14], spaced by ∼1 THz from the pumps. Our numerical simulations of the scan, shown in fig. 3b, provide good agreement with the experiment and help to shed some light on the comb formation mechanism. The initial multiple FWM creates a narrow coherent comb around the pump lines. Changing the pump frequency detuning leads to the emergence of spontaneous MI gain lobes, under which multiple cavity modes are oscillating [22], which degrades the coherence. In addition, the MI induces sub-combs (fig. 3d.), whose line spacing matches that of the initial Kerr comb, with a frequency offset [23]. These sub-combs can be still synchronized, under appropriate detuning conditions, to form one globally coherent comb [24], which is shown in fig. 3e. This optimal Brillouin pumps spacing is commensurate with the cavity's FSR, which provides a wider stable Kerr comb spectrum and allows a spectral broadening of around 6 THz. Interestingly, the desynchronization does not significantly affect the comb symmetry, as in the normal dispersion case, but rather the strength of the MI lobes and the offset mismatch of the subcombs. When the pump detuning is strongly mismatched, the cascaded FWM becomes less efficient and creates a narrow Kerr comb spectrum, as shown in fig. 3a, with a bandwidth less than 1 THz. The excellent coherence of the synchronized Kerr comb was confirmed by beating a selected comb line (−10) and an auxiliary tunable narrow-linewidth laser (see inset in fig. 3e). Indeed, the intrinsic properties of SBS induce a linewidth-narrowing of the Stokes laser [25, 26]. The combs have also been characterized in the time domain. Figure 3f shows the temporal intensity profiles of the pulse trains corresponding to the combs in figs. 3c,e. Our numerical prediction (fig. 3g) of the intracavity temporal intensity profile corresponding to the wider comb shows good agreement with the experimental data. The broad synchronized Kerr comb spectrum corresponds to stable MI patterns emerging on top of a flat-top modulation pattern (blue curve). The fact that these patterns can be captured with a sampling oscilloscope further validates the coherence and stability of the comb. When the MI sub-combs are mismatched and incoherent, these additional patterns are smeared (green curve). In the strongly mismatched driving case, the pulse train shows little deviation from a sinusoidal pattern (red curve). Note that the soliton state could not be reached in our experiments, due to the inherent detuning limitation imposed by mode-hopping [19].

3. CONCLUSION

In conclusion, we have experimentally and numerically explored the dynamics of Brillouin – Kerr comb formation in nonlinear fiber cavities. The dual-pumping configuration provides an easy way to harness Kerr combs in fiber laser cavities and is an interesting alternative to traditional methods. The key feature of this scheme is the ability to easily change and reconfigure the dispersion as well as the comb spacing, which is determined by the spacing between the two Brillouin pumps. We demonstrate the key importance of these two quantities in the emergence, shape, and dynamics of the Kerr comb states. The comb repetition rate can also be varied across a wide range, which is desirable in applications such as microwaves generation or telecommunications. Finally, this architecture opens perspectives for operation in new spectral windows using higher confinement waveguides

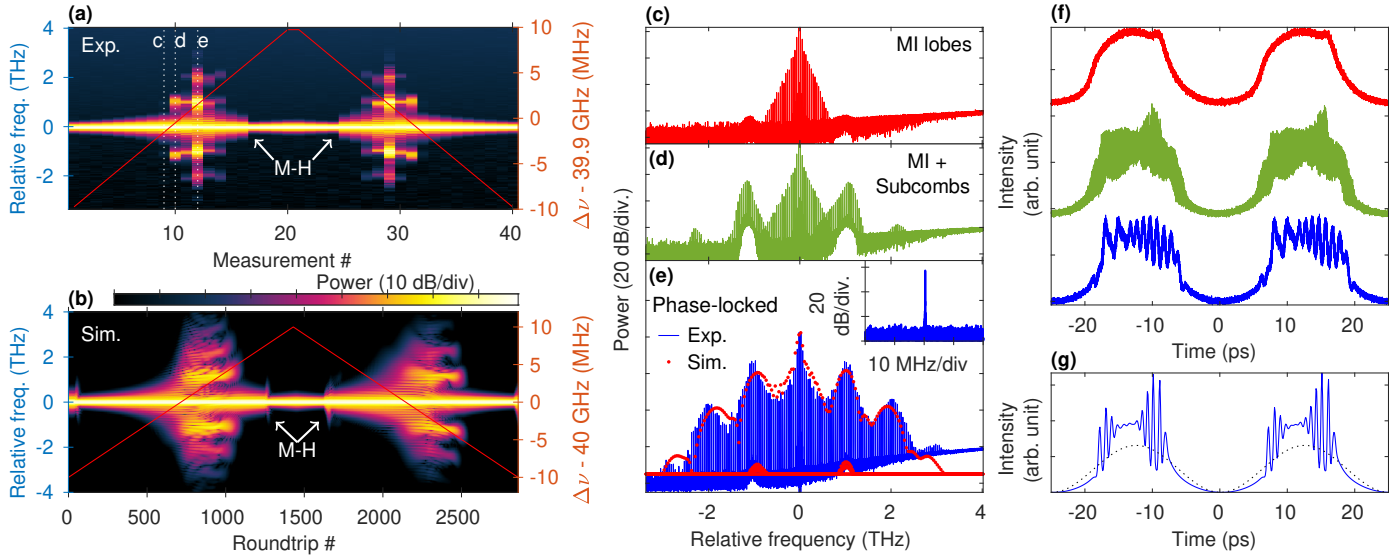

Fig. 3. Anomalous net dispersion regime. **(a)** Experimental recording of the comb spectrum evolution with $\Delta\nu$, at a fixed injected optical power of 535 mW. M-H : Mode Hopping. **(b)** Numerical modeling of the Kerr combs evolution depending on $\Delta\nu$. **(c)** Kerr comb spectrum showing the growth of spontaneous MI around the initial comb. **(d)** Illustration of the sub-comb formation on the MI gain lobes. These comb are offset from the center comb. **(e)** Broadest phase-locked comb with minimized spontaneous modulation-instability, when matching the pump spacing with a FSR-multiple. The sub-combs are synchronized, to form a single coherent comb. Inset: Beatnote signal between the comb and an auxiliary narrow-linewidth laser around 1555 nm (resolution bandwidth 30 kHz). **(f)** Experimental temporal intensity profiles of the generated pulse train corresponding to the cases reported in (c) to (e). **(g)** Numerical simulation of intra-cavity temporal intensity profile corresponding to the comb reported in (e).

and new specialty fiber materials with strong nonlinearity.

Funding. The authors acknowledge support from French program "Investments for the Future" operated by the National Research Agency (EIPHI Graduate School, contract ANR-17-EURE-0002), and from Région Bourgogne Franche-Comté and European Regional Development Fund.

Disclosures. The authors declare no conflicts of interest.

REFERENCES

1. S. A. Diddams, K. Vahala, and T. Udem, Science **369**, eaay3676 (2020).
2. A. B. Matsko, A. A. Savchenkov, W. Liang, V. S. Ilchenko, D. Seidel, and L. Maleki, Opt. Lett. **36**, 2845 (2011).
3. J. Fatome, S. Pitois, C. Fortier, B. Kibler, C. Finot, G. Millot, C. Courde, M. Lintz, and E. Samain, Opt. Commun. **283**, 2425 (2010).
4. G. Millot, S. Pitois, M. Yan, T. Hovhannisyan, A. Bendahmane, T. W. Hänsch, and N. Picqué, Nat. Photonics **10**, 27 (2016).
5. T. J. Kippenberg, R. Holzwarth, and S. A. Diddams, Science **332**, 555 (2011).
6. T. Herr, V. Brasch, J. D. Jost, C. Y. Wang, N. M. Kondratiev, M. L. Gorodetsky, and T. J. Kippenberg, Nat. Photonics **8**, 145 (2014).
7. W. Liang, A. B. Matsko, A. A. Savchenkov, V. S. Ilchenko, D. Seidel, and L. Maleki, "Generation of Kerr combs in MgF2 and CaF2 microresonators," in *2011 Joint Conference of the IEEE International Frequency Control and the European Frequency and Time Forum (FCS) Proceedings,* (IEEE, San Francisco, CA, USA, 2011), pp. 1–6.
8. Y. Bai, M. Zhang, Q. Shi, S. Ding, Y. Qin, Z. Xie, X. Jiang, and M. Xiao, Phys. Rev. Lett. **126**, 063901 (2021).
9. I. H. Do, D. Kim, D. Jeong, D. Suk, D. Kwon, J. Kim, J. H. Lee, and H. Lee, Opt. Lett. **46**, 1772 (2021).
10. Q. Li, Z.-x. Jia, Z.-r. Li, Y.-d. Yang, J.-l. Xiao, S.-w. Chen, G.-s. Qin, Y.-z. Huang, and W.-p. Qin, AIP Adv. **7**, 075215 (2017).
11. Y. Huang, Q. Li, J. Han, Z. Jia, Y. Yu, Y. Yang, J. Xiao, J. Wu, D. Zhang, Y. Huang, W. Qin, and G. Qin, Optica **6**, 1491 (2019).
12. W. Xiong, C. Yao, P. Li, Y. Wang, and F. Zhu, IEEE Photonics J. **14**, 1 (2022).
13. X. Zhang, Z. Jia, Y. Huang, J. Wu, T. Wang, Y. Chen, Y. Yu, Y. Yang, J. Xiao, W. Qin, Y. Huang, and G. Qin, J. Light. Technol. **41**, 1820 (2023).
14. D. Ceoldo, A. Bendahmane, J. Fatome, G. Millot, T. Hansson, D. Modotto, S. Wabnitz, and B. Kibler, Opt. Lett. (2016).
15. A. Bendahmane, J. Fatome, C. Finot, G. Millot, and B. Kibler, Opt. Lett. **43**, 4449 (2018).
16. M. Deroh, B. Kibler, H. Maillotte, T. Sylvestre, and J.-C. Beugnot, Opt. Lett. **43**, 4005 (2018).
17. G. Danion, L. Frein, D. Bacquet, G. Pillet, S. Molin, L. Morvan, G. Ducournau, M. Vallet, P. Szriftgiser, and M. Alouini, Opt. Lett. **41**, 2362 (2016).
18. L. C. Sinclair, J.-D. Deschênes, L. Sonderhouse, W. C. Swann, I. H. Khader, E. Baumann, N. R. Newbury, and I. Coddington, Rev. Sci. Instruments **86**, 081301 (2015).
19. E. Lucas, M. Deroh, and B. Kibler, "Dynamic Interplay Between Kerr Combs and Brillouin Lasing in Fiber Cavities," (2022). ArXiv:2212.08534 [physics].
20. G. P. Agrawal, *Nonlinear Fiber Optics 6th ed.* (Academic Press, 2019).
21. B. Garbin, Y. Wang, S. G. Murdoch, G.-L. Oppo, S. Coen, and M. Erkintalo, The Eur. Phys. J. D **71**, 240 (2017).
22. A. Bendahmane, J. Fatome, C. Finot, G. Millot, and B. Kibler, Opt. Lett. **42**, 251 (2017).
23. T. Herr, K. Hartinger, J. Riemensberger, C. Y. Wang, E. Gavartin, R. Holzwarth, M. L. Gorodetsky, and T. J. Kippenberg, Nat. Photonics **6**, 480 (2012).
24. P. Del'Haye, K. Beha, S. B. Papp, and S. A. Diddams, Phys. Rev. Lett. **112**, 043905 (2014).
25. A. Debut, S. Randoux, and J. Zemmouri, Phys. Rev. A **62**, 023803 (2000).
26. S. Gundavarapu, G. M. Brodnik, M. Puckett, T. Huffman, D. Bose, R. Behunin, J. Wu, T. Qiu, C. Pinho, N. Chauhan, J. Nohava, P. T. Rakich, K. D. Nelson, M. Salit, and D. J. Blumenthal, Nat. Photonics **13**, 60 (2019).